The Meteoritical Society

Meteoritics & Planetary Science 1–15 (2025)
doi: 10.1111/maps.14313

The solar system Fe/Mg ratio

D. S. BURNETT[1]*, A. J. G. JUREWICZ[2], D. S. WOOLUM[3], Y. GUAN[1], V. S. HEBER[4,5], R. HERVIG[6], M. HUMAYUN[7], K. D. MCKEEGAN[4], L. R. NITTLER[2,8], C. T. OLINGER[9], D. B. REISENFELD[10], and J. WANG[8]

[1]Division of Geological and Planetary Sciences, California Institute of Technology, Pasadena, California, USA
[2]Center for Meteorite Studies, Arizona State University, Tempe, Arizona, USA
[3]Department of Physics, California State University, Fullerton, California, USA
[4]Department of Earth, Space, and Planetary Sciences, UCLA, Los Angeles, California, USA
[5]Division for Radiation Safety and Security, Paul Scherrer Institut, Villigen PSI, Switzerland
[6]School of Earth & Space Exploration, Arizona State University, Tempe, Arizona, USA
[7]National High Magnetic Field Laboratory & Department of Earth, Ocean & Atmospheric Science, Florida State University, Tallahassee, Florida, USA
[8]Department of Terrestrial Magnetism, Carnegie Institute of Washington, Washington, DC, USA
[9]GET, Inc, Germantown, Maryland, USA
[10]Los Alamos National Laboratory ISR-1, Los Alamos, New Mexico, USA

***Correspondence**
D. S. Burnett, Division of Geological and Planetary Sciences, California Institute of Technology, Pasadena, CA 91125, USA.
Email: dburnett@caltech.edu

(Received 04 December 2023; revision accepted 07 January 2025)

Abstract–Solar wind Fe and Mg fluences (atoms/cm^2) were measured from Genesis collectors. Fe and Mg have similar first ionization potentials and solar wind Fe/Mg should equal the solar ratio. Solar wind Fe/Mg is a more valid measure of solar composition than CI chondrites and can be measured more accurately than spectroscopic photospheric abundances. Mg and Fe fluences analyzed in four laboratories give satisfactory agreement. Si and diamond-like carbon collector fluences agree for both elements. The Mg and Fe fluences are $1.731 \pm 0.073 \times 10^{12}$ and $1.366 \pm 0.058 \times 10^{12}$ atoms/cm^2. All plausible sources of errors down to the 1% level are documented. Our value for the solar system Fe/Mg, 0.789 ± 0.048 agrees within 1 sigma errors with CI chondrites, spectroscopic photospheric abundances, and with the solar wind data from the ACE spacecraft. CI samples from asteroid Ryugu give Fe/Mg in agreement with Genesis and meteoritic CI samples despite very small sample sizes. The higher accuracy of the Genesis solar Fe/Mg permits a comparison with chondritic Fe/Mg at the 10% level. Intermeteorite Fe/Mg averages differ among the main C chondrite groups but are within, or very close to, the ±1 sigma Genesis solar Fe/Mg.

INTRODUCTION

Solar elemental abundances are important to planetary science. Most models assume that, except for He and Li, the elemental composition of the solar photosphere is equal to that of the solar nebula from which planetary materials formed; for elemental abundances, there is no confirmed contradictory evidence. Adopted solar abundances for nonvolatile elements are based on analyses of photospheric absorption lines or by proxy from Ivuna type (CI) carbonaceous chondrites. The Genesis spacecraft collected and returned samples of the solar wind (SW) for laboratory analyses (Burnett, 2013; Burnett et al., 2019). Elemental and isotopic abundances of SW captured by Genesis have been successfully measured despite the crash of the re-entry capsule. The goal of Genesis is, whenever possible, to use SW composition to determine the average solar isotopic

and elemental compositions at levels of precision required for 21st-century planetary science. The quantitative goals for Genesis elemental analyses are to improve solar abundances by a factor of 3 from photosphere spectroscopic values.

The solar photosphere is the outer portion of the Sun from which visible light escapes. Except for D, ^{3}He, and Li, compositional changes due to thermonuclear reactions have not affected the photosphere. Despite major improvements, spectroscopic measurements of the photosphere (e.g., Asplund et al., 2021) do not have the element coverage and accuracy needed for many cosmochemical applications. As a proxy for solar composition, planetary scientists use analyses of CI chondrites (e.g., Lodders, 2021; Palme et al., 2014). CI chondrites are, moreover, very complicated rocks (e.g., McSween, 1993) with many opportunities for elemental fractionation during their formation processes. Thus, CI abundances are a *valid* representation of solar composition *only* to the extent that they agree with the spectroscopic abundances. The *true* uncertainties in adopted abundances are not the high analytical accuracy of the CI analyses but the larger uncertainties in the spectroscopic measurements.

Differences in CI-normalized abundances among C chondrite groups (as well as among H chondrites, which have similar major element composition) can be both small, around 10% or less for some elements (Palme et al., 2015), and large, factors of 2–3 for volatile elements (Palme et al., 2014). In the case of factors of 2–3 differences, 10%–20% errors in the adopted nebular elemental reference abundances may not significantly impede interpretations, but the spectroscopic photospheric abundances of many volatile trace elements have much larger errors. Genesis solar wind abundances are potentially more valid than CI abundances and more accurate than spectroscopic photospheric abundances.

For Genesis SW elemental abundances, Mg is the logical reference element. The Mg fluence (atoms/cm^2) is high and can be analyzed accurately by many techniques. Although Mg-normalized abundances are available for seven elements from Heber et al. (2021), these do not include Fe. Here, we report analyses of Fe/Mg; the fluence ratio is shown to be equal to the solar abundance ratio. Fe is an important rock-forming element and of high cosmochemical importance. The high Genesis Fe fluence enables accurate fluences, and an accurate Fe/Mg ratio, allowing for close comparisons with other measurements of meteoritic and solar Fe/Mg.

ANALYTICAL METHODS

Solar wind Mg analyses were made using the ASU 6f, the CIW 6f, the Caltech 7f, and the UCLA 1270 Cameca secondary ion mass spectrometry (SIMS) instruments. For both Mg and Fe, two collector materials were used: silicon (Si) and diamond-like carbon on silicon (DLC) (Jurewicz et al., 2003). All samples analyzed were bulk solar wind (Burnett, 2013).

Implanted SW depths are shallow (<1 micron). All analyses were performed using SIMS front side depth profiling on a small area (square rasters 100–200 microns on a side), starting at the SW collection surface, and sputtering into the sample. Accordingly, surface contamination is an issue. Ideally, contaminating films needed to be removed, and particulates either removed or avoided. Before allocation, at the JSC Genesis Curatorial Facility, samples underwent megasonic cleaning in ultra-high purity water to remove loose particulates: This is very effective at removing dust from the Genesis re-entry crash. Variable cleaning procedures were used (Burnett et al., 2019, p. 1107), with varying degrees of effectiveness, but, with the exception of sample 60490 (discussed below), none of these removed any of the implanted solar wind. Occasionally, for Mg profiles in Si, a distorted depth profile would be measured and rejected under the assumption that a submicron particulate was accidentally incorporated into the analyzed area. The rejection rate varied with both collector type and sample but was generally less than 1 per five analyses.

Mg and Fe were analyzed as positive secondary ions. Analysis conditions changed with time and with material being analyzed as we improved our methods. An O_2^+ primary beam (5 kV or 8 kV impact energy) was always used because of the higher depth resolution compared to that for O^- and, more importantly, because of smaller transients in the near surface region. Transients are the time for both sputtering rate and counting rates to reach sputtering steady state. Electron multiplier (EM) pulse counting detectors were used to count solar wind ions and $^{12}C^+$ matrix ions from DLC. For silicon collectors, ^{28}Si matrix ion currents were measured with a Faraday Cup (FC). Sputtering rates were generally 0.1–0.5 nm/sec using 20–100 nA primary currents. As discussed below, for the analysis of Si collectors leaking or "bleeding" O_2 into the analysis chamber was found to reduce transients for the Si matrix. Sufficient mass resolving power was used to cleanly resolve $^{24}Mg^+$ from C_2^+.

After exploration of appropriate run conditions, analytical protocols were standardized and maintained in all analyses to maximize reproducibility. In most cases, samples were analyzed in the center hole of the same 1-hole mount with no gaps or broken edges showing, and all analyses were taken at least 1.5 mm away from the ridge interface of sample and holder. Multiple profiles were obtained per analysis session with flight sample analyses usually bracketed between reference ion-implant standard analyses.

Quantifying SW Depth Profiles

The usual materials science approach (Wilson et al., 1989) for obtaining fluences of an implanted trace isotope, i (e.g., ^{25}Mg or ^{54}Fe), by depth profiling in a collector composed of an element with a matrix isotope, m where m is ^{28}Si or ^{12}C, is based on the RSF (relative sensitivity factor):

$$n_i(x) = \mathrm{RSF}^* \{C_i(x)/C_m\} \quad (1)$$

where $n_i(x)$ is the concentration (SW atoms/cc) of atom i as a function of depth x, and C is the background-corrected counting rate of i, which for solar wind ions is also a function of depth. C_m is the matrix ion counting rate (^{28}Si or ^{12}C).

The fluence of i is the depth integral:

$$\begin{aligned}\mathrm{fluence}\left(i\ \mathrm{atoms/cm^2}\right) &= \int [n_i(x)\mathrm{d}x] \\ &= \mathrm{RSF} \int [C_i(x)/C_m]\mathrm{d}x\end{aligned} \quad (2a)$$

or, since the data are determined as a time sequence, Equation (2a) is equivalent to:

$$\mathrm{fluence} = \mathrm{RSF}^* \int [C_i(x)/C_m]^* \, S \, \mathrm{d}t \quad (2b)$$

Instrument conditions were tuned to maintain a constant sputtering rate, $S = \mathrm{d}x/\mathrm{d}t$. S is determined as crater depth/total run time where the crater depth is measured by profilometry. Depth integrals are determined from the surface to a depth where the implant concentration becomes negligible. Since the same instrument was used for measuring pit depths on sample and standard, only the precision of the pit depth measurement contributes to the fluence error. Replicate analyses of pits give a reproducibility of about 1%.

When samples and standards are measured as close in time as possible, the above equations simplify to:

$$\begin{aligned}\text{SW fluence} = \text{implant std fluence} \times [\text{SW depth integral}/ \\ \text{standard depth integral}]\end{aligned} \quad (3)$$

SW fluences were calculated relative to implant standards, using Equations (2a) or (3) with the RSF obtained from the same equation applied to a measured depth profile from an implant standard with known fluence. The implant standard is usually an unflown control sample of flight material implanted with a known fluence of a minor isotope of the SW element of interest. Although the solar wind ions were counted with an EM, and the matrix element usually with an FC, an FC to EM intercalibration is not necessary because reference implants and SW were measured under the same conditions; therefore, the scaling factor cancels. For Mg analyses, implanted ^{25}Mg was used to obtain the RSF, and then, the solar wind fluence was determined from the ^{24}Mg depth profile measured in the flown samples. For the case of Fe, ^{54}Fe or ^{56}Fe implants were used, with solar wind ^{56}Fe profiles measured in the flown collectors.

RESULTS

Detailed documentation of fluence measurements and associated errors are given in supporting online appendices. More complete documentation, especially on how errors were estimated, is available in expanded versions of these appendices from D. Burnett or A. Jurewicz. Appendix A gives a table of contents (Appendix List).

External Versus Internal Standards

Materials science depth profiling is based on "external standardization" in which an implant standard is a separate sample, analyzed separately (Wilson et al., 1989). A derived externally standardized solar wind (SW) fluence is thus based on the measurement of separate depth profiles from the Genesis sample and from the implant standard, ideally measured under exactly the same analytical conditions. Greater accuracy was obtained by implanting ^{25}Mg or ^{54}Fe directly into flight samples, creating a "flight implant internal standard" so that fluences are derived from a single depth profile. Fluences derived from both external and internal standardization are reported here.

MG

Mg Implant Standards

The nominal standard implant fluences reported by the vendor are not sufficiently accurate for Genesis applications (Heber et al., 2014). Independent calibration of the implant fluence is required, but this is feasible. Table 5 in Burnett et al. (2015) shows that five different Mg implants have been calibrated with differences of up to 24% below the nominal fluences. All solar wind Mg and Fe fluences reported here are based on calibrated implants; a list is given in Appendix B.

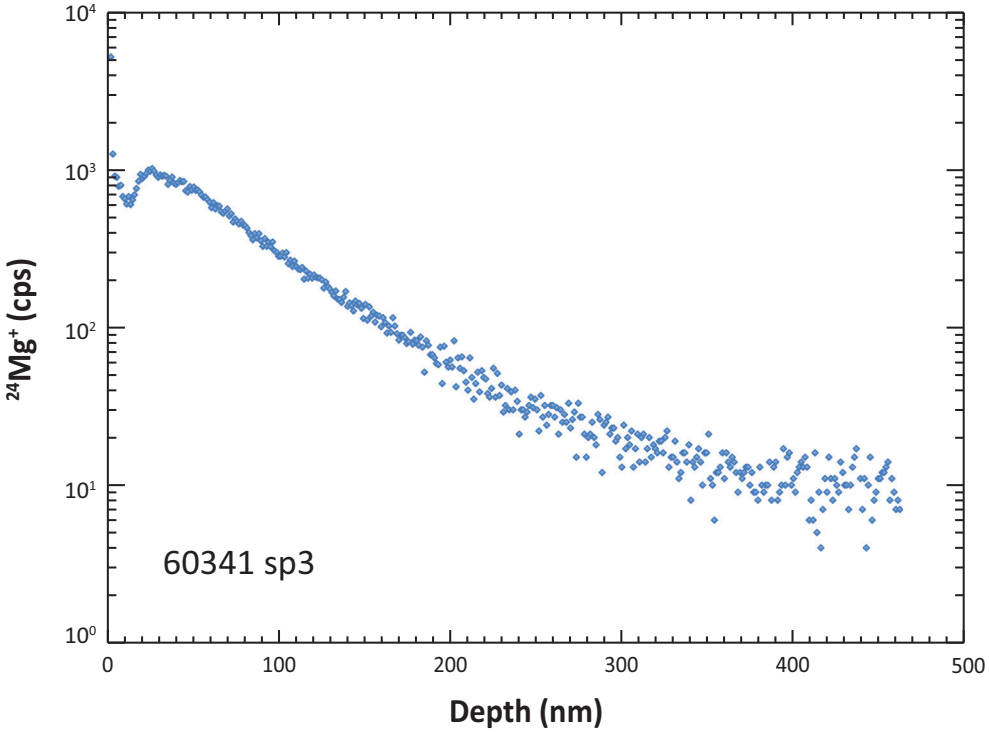

FIGURE 1. Typical solar wind ^{24}Mg depth profile in Si collector. The first 10 nm is unusable because of surface contamination and transients. Background is reached beyond 400 nm. Signal to noise is excellent. An accurate Mg solar wind fluence is given by the depth integral of the background-corrected ^{28}Si-normalized ^{24}Mg counting rate.

Mg Fluences from Si Collectors (Appendix C)

Depth Profiles

Figure 1 shows a typical ^{24}Mg counting rate depth profile. The decreasing Mg ion intensity from the surface is a mixture of transient behavior and ion-beam-mixed surface contamination. The minimum in the profile around 10 nm represents the transition from a decreasing contamination profile to an increasing SW profile. The SW profile peaks at about 20 nm and drops off relatively slowly with depth until reaching the background level beyond 400 nm. Overall signal to background is excellent. At any one instant, the SW has a constant speed, but over the course of the 27-month Genesis exposure, the speed of the SW plasma cloud varies, causing implantation depth variations resulting in a broad implantation profile because implantation depth depends on ion energy. The breadth is a convolution of the intrinsic dispersion in stopping depths at constant velocity and spread due to variation in SW speed. Beyond around 200 nm, the profile is exponential, which can be used to make a small "tail correction" for the unanalyzed deep tail of the SW profile beyond 400 nm.

In general, for all depth profiles, the first portion of the depth profile is not measured quantitatively because of transients and surface contamination. The "main" part of the depth integral has a lower limit ("start main depth") at depths significantly greater than when steady state sputtering has been achieved and well into the rising part of the profile where contamination should be negligible. Surface corrections from the surface to the start main depth are made by fitting the portions of the measured profiles more shallow than the peak to a theoretical depth profile based on the SRIM software (Ziegler et al., 2010). The total depth integral is the sum of surface + main + tail integrals. Errors from the surface and tail corrections have been assessed in detail (see Appendices). Surface corrections and errors are comparable for Mg and Fe, so no significant bias in the Fe/Mg ratio from different amounts of contamination is present.

As an internal standard, flight sample 60341 was implanted with $9.17 \pm 0.38 \times 10^{11}$/cm^2 ^{25}Mg ions at 100 keV. The 60341 ^{25}Mg implant fluence was calibrated by intercomparing profiles from a piece of flight spare Si K7A (co-implanted along with 60341) with Si sample CZ4A. In turn, CZ4A was co-implanted with an NIST 617 glass of known Mg concentration (Burnett et al., 2015). SIMS analysis of the implant profile in the NIST glass established the ^{25}Mg implant fluence of CZ4A as $2.63 \pm 0.08 \times 10^{13}$/cm^2. In this bootstrapping manner, a series of implant standards were generated based on the well-calibrated NIST glass. The 60341 ^{25}Mg implant

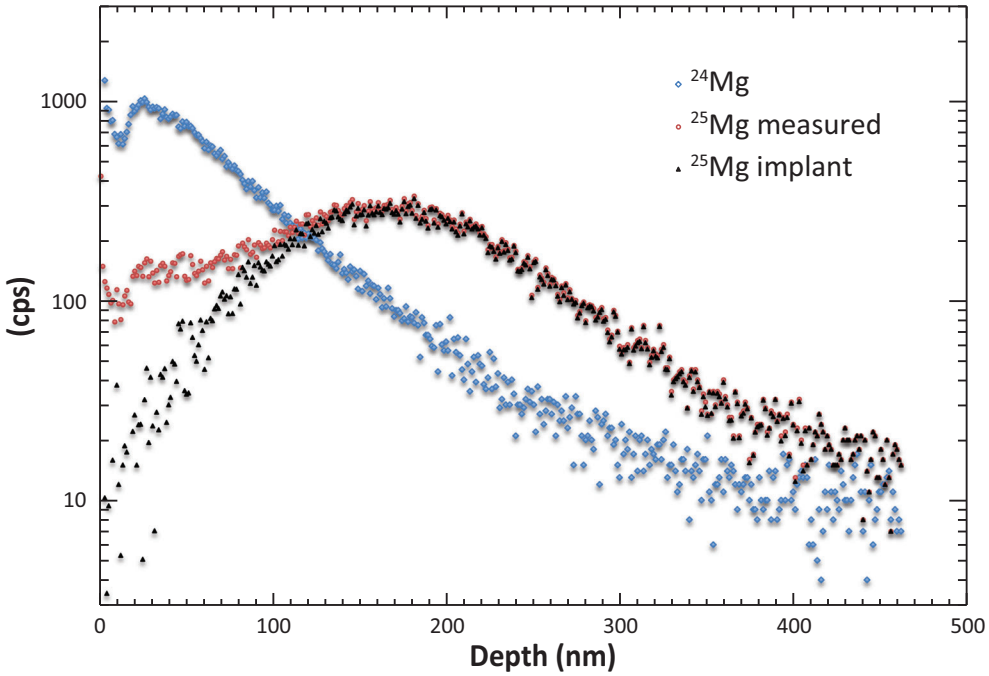

FIGURE 2. Measured counting rate ^{24}Mg and ^{25}Mg depth profiles from an ^{25}Mg implant into sample 60341. The measured ^{24}Mg profle is shown as diamonds. Implant ^{24}Mg is negligible. The measured ^{25}Mg profile (dots) requires correction for solar wind ^{25}Mg, but this can be accurately made, as shown in the derived ^{25}Mg implant profile (triangles).

energy and fluence were chosen to give a depth profile deeper than, but with a similar fluence as expected for SW ^{24}Mg. A summary of implant standards used is given in Appendix B.

Figure 2 shows measured depth profiles for implanted ^{25}Mg and SW ^{24}Mg in 60341. The implant ^{25}Mg ion beam was extracted, and mass analyzed from an ion source using terrestrial Mg (^{24}Mg/^{25}Mg = 7.9), but the "accidental" implanted impurity ^{24}Mg is small: ^{24}Mg/^{25}Mg = 1.88×10^{-3}. Given the relative implant and solar wind fluences and depth distributions, the contribution of the laboratory implanted ^{24}Mg to the 60341 solar wind ^{24}Mg is negligible and has been ignored. However, as can be seen in Figure 2, there is a significant contribution of solar wind ^{25}Mg to the measured implant ^{25}Mg profile causing the flat part of the profile nearer to the surface than 100 nm. Accurate corrections for the SW "contamination" of the measured ^{25}Mg implant standard profile can be made based on the measured ^{24}Mg profile, giving the corrected ^{25}Mg implant profile in Figure 2 (Appendix C).

Depth Integrals

At depths greater than about 13 nm, the background-corrected ^{24}Mg profile is pure SW. From the surface to about 13 nm, the measured ^{24}Mg is a mixture of SW and contamination distorted by transient effects. A surface correction is required for this portion of the profile (Appendix C).

Primary ion currents were very stable during internal standard profile measurements. Here, the SW ^{24}Mg fluence is simply the implant fluence times the ratio of the solar wind ^{24}Mg and implant ^{25}Mg counting rate depth integrals plus a small instrumental mass fractionation (IMF) correction estimated as -1.0 ± 0.5%/amu based on analyses of silicate materials, where the minus sign means light isotope enrichment. In all cases, for both implant standard and SW, the total integral is the sum of three parts: surface + "main" + tail. For the best (internally standardized) profiles, the main part is greater than 90% of the total. For all Mg profiles accepted for a fluence calculation, the fraction of the total integral represented by the clean main portion ranges from 83% to 94%.

The SW ^{24}Mg surface correction integral in the first 10–15 nm (Appendix C) amounts to 6%–8% of the total 60341 fluences. The tail correction for the unmeasured deep part ("tail") of the 60341 ^{24}Mg profiles is small (0.2%–0.4%). Similar surface and tail corrections for the ^{25}Mg implant depth profiles are more complicated, but these are small sources of error; the corrections to the ^{25}Mg depth integral are approximately 0.6%–0.8% for the surface and 1.7%–1.9% for the implant tail (Table C3).

Mg Fluences

Figure 3 displays individual profile Mg fluence analyses arranged sequentially according to date of analysis in what can be regarded as a "learning curve".

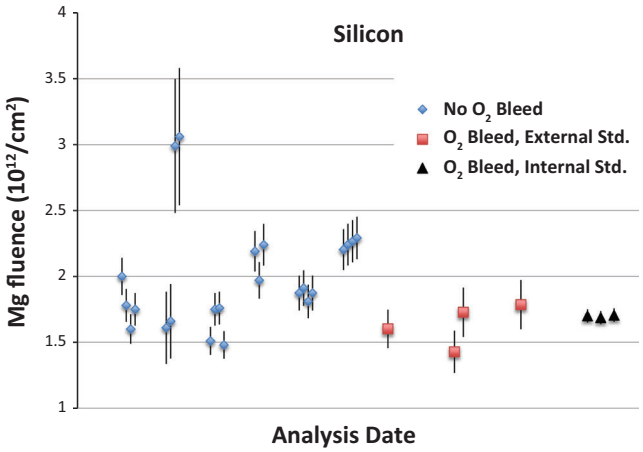

FIGURE 3. "Learning curve" for Mg. Fluence reproducibility was poor before use of O_2 gas bleed, but good results were obtained after use, for both internal and external standardized profiles. Error bars (1 sigma) are precision. Errors common to all points are not included. Three externally standardized profile analytical sessions are shown (A, B, C. Appendix C, Table C1).

Initially, externally standardized fluences gave poor reproducibility, both for implant standards and for solar wind Mg profiles. Part of this was lack of standardization of analytical conditions, but for reasons not completely understood, the greatest improvement in reproducibility occurred when we incorporated the O_2 flooding in the analyses. All fluences on Figure 3 are based on calibrated implants.

Fluences from the three 60341 internal standard profiles are in excellent agreement (Table 1) with a standard deviation of 0.6%. The precision of the internal standard fluences is 3.1%, with error bars comparable to the size of the symbol in Figure 3.

External standard analyses with O_2 flooding were made in three sessions (A, B, C) earlier than the internal standard analyses (Table C). These were not made under the standardized conditions later adopted, and fluences have larger errors, order 10%. As Figure 3 and Table 1 show, the measured fluences for three of the four profiles agree within 1 sigma errors with the more precise fluence determined from the internal standard analyses. The fourth is low by 2 sigma.

A large number of sources of error at the percent level have been studied in some detail. Table C4 gives a detailed breakdown of the sources of error for the internal standard analyses.

Mg Fluence from Si collectors, Summary

Table 1 is the total summary of the adopted individual profile solar wind Mg fluence data. To make the appropriate comparisons, error bars are precision, omitting common sources of error to all data, for example, the Mg concentration of the primary NIST standard. For Si collectors, we adopt the average 60341 internal standard fluences as the final Mg fluences from Si collectors: $1.698 \pm 0.053 \times 10^{12}$ atoms/cm^2 (precision). We do not adopt an error of the mean because of the possibility of unrecognized errors.

Our frontside Si collector fluences agree with the backside Si Mg fluence of Heber et al. (2021) (Table 1).

TABLE 1. Genesis solar wind Mg fluences.[a]

	Mg fluence	Error[b]
Si collectors		
Internal Standard[c]		
60341–01	1.700	0.061
60341–02	1.687	0.061
60341–03	1.706	0.062
External Standard[d]		
A 20732–1-5	1.60	0.15
B 20732–1-1	1.43	0.16
B 20732–1-2	1.73	0.19
C 20733–1-2	1.79	0.19
Heber et al., 2021[e]	1.761	0.044
DLC collectors		
Internal Standard[c]		
60246–2	1.702	0.071
60246–3	1.768	0.057
External Standard[d]		
E Average 20732–2[f]	1.734	0.059
D 60065 average[g]	1.86	0.28

[a]Units of 10^{12} atoms/cm^2.
[b]Sources of error common to all analyses omitted. See text Adopted Solar Wind Mg Fluence Section.
[c]Estimated average precision of single profile (Table C4).
[d]Letters refer to analysis sessions (Appendix C for Si; Figure 4 for DLC).
[e]Correction and error added for effect of H on Mg sensitivity (Section C7).
[f]Average of 11 analyses (Jurewicz et al., 2021; Appendix D1).
[g]Average of three profiles (Table D2-2-4).

Mg Fluence from Diamond-Like-C (DLC) Collectors

The calculation of solar wind Mg fluences from ^{24}Mg SIMS depth profiles in DLC is basically the same as described in the above Mg Fluences from Si Collectors Section and Appendix C for Si collectors; however, there are significant differences in detail. Complete descriptions of the data processing are given in Appendices D1 and D2. Figure 4 shows the DLC learning curve analogous to Si collectors (Figure 3). Measured external standard fluences showed lot of scatter initially until we learned how to standardize conditions to obtain more reproducible results. In several of the early analysis sessions, the agreement in replicate solar wind analyses is good, but the large error bars reflect irreproducibility with the measured implant

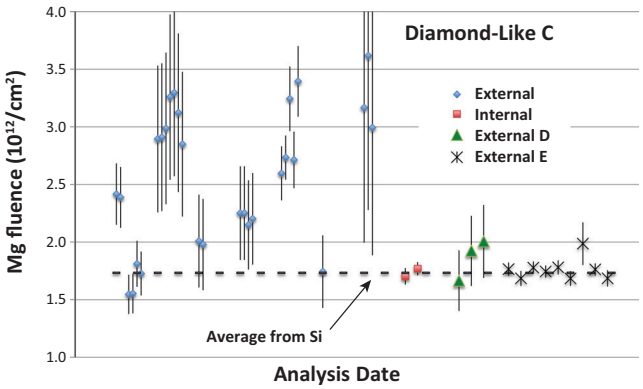

FIGURE 4. "Learning curve" for diamond-like C (DLC) collectors. Initially, reproducibility was poor, until control of DLC inhomogeneities was established (Jurewicz et al., 2021). Error bars (1 sigma) are precision. Errors common to all points are not included.

standards. The irreproducibility can be understood by variations in DLC conductivity (Jurewicz et al., 2021, fig. 6 discussion). All fluences in Figure 4 are based on calibrated implants, but as with Figure 3, we have not made a major effort to understand the scatter in the early data. We only use the results of the final 3 sessions: the internal standard, and external standard sessions D and E. Sessions D and E analyses were made using highly controlled analytical conditions with all analyses being made in the same sample mount. Session E is discussed in detail in Appendix D1. The 60246 internal standard and session D are in Appendix D2. Figure 4 shows that the session D and, especially, session E analyses have less scatter than the analyses prior to the flight implant internal standard. The error bars (1 sigma) in Figure 4 are the relative precision of the different analyses shown; sources of error common to all points in the figure are not included.

20732–2 Session E

The smaller errors in the 20732–2 analyses are due to a major effort to understand the effects of DLC inhomogeneity (Jurewicz et al., 2017, 2020, 2021) which resulted in reproducible fluences for the Session E 20732–2 data: (1) Variations in the implant standard depth integrals (i.e., sensitivity factors) were found to be correlated with C_2/C matrix ion intensity variations. This correlation, coupled with the measured C_2/C of the 20732–2 profiles, gave accurate sensitivity factors. (2) By using a calibrated two isotope ($^{25}Mg + {}^{26}Mg$) implant standard, large, and somewhat variable, instrumental mass fractionation (circa 40 permil/amu) was demonstrated. (3) The implant standard has a previously unrecognized, relatively deep, ^{24}Mg contamination profile. Accurate surface corrections were possible for the 20732–2 solar wind profiles (Section D1-9) based on theoretical SRIM profiles (Olinger et al., 2018; Ziegler et al., 2010).

The 20732–2 session E data are independently processed here (Appendix D1) using similar, but not exactly the same, procedures as Jurewicz et al. (2021). The individual profile fluences (Table D1-4) are in excellent agreement. The average of nine profiles is given in Table 1.

The good SRIM fits to the 20732–2 DLC solar wind profiles are illustrated in Figure D1-8. Unlike Si, SRIM gives excellent fits to both the implant standard and solar wind profiles.

Internal Standard 60246

DLC sample 60246 was implanted together with 60341 Si, with ^{25}Mg at a deeper depth, but with a comparable fluence as the SW depth profiles (Figure D2-1-1). Fluence calculations (Appendix D2-1) are essentially the same as the internal standard Si depth profiles (Figure 2). Corrections for implant ^{24}Mg are negligible, but small corrections to the ^{25}Mg implant by solar wind ^{25}Mg are required. The internally standardized analyses minimize fluence errors from DLC inhomogeneity. The implant ^{25}Mg was deliberately made much deeper than the solar wind ^{24}Mg. However, C_2/C is observed to be uniform in a given profile, although variable among profiles separated by a few hundred microns, implying that sensitivity factors are constant in any one profile.

Fluences from two 60246 profiles agree within errors, differing by 3.9%. The average 60246 fluence is $1.735 \pm 0.047 \times 10^{12}$ atoms/cm^2.

External Standard 60065 (session D)

These analyses were done under tightly controlled analytical conditions (Appendix D2-2), but C_2/C measurements were not made; thus, fluence errors are large due to DLC inhomogeneities. Session D data are not used in the final value for the solar wind Mg fluence. Three profiles were measured with fluences (in units of 10^{12}atoms/cm^2) ranging from 1.66 to 2.01 (Table D2-2-4; Figure 4), but 1 sigma error bars overlap and each fluence agrees within errors of that for internal standard 60246. The average 60065 fluence is given in Table 1.

DLC Solar Wind Mg Fluence

Summarizing: the work of Jurewicz et al. (2017) and Jurewicz et al. (2021) has demonstrated that the DLC SIMS sensitivity factor variations (±10%–15% based on 60065. Appendix D2-2) can be corrected based on measured C_2/C matrix counting rate ratios. Good precision is obtained for 11 external standard profiles for sample 20732–2 (Figure 4; Tables 1 and D1-4). Use of an ^{25}Mg implant internal standard also compensates for

sensitivity variations, and agreement well within errors is found for samples 60246 (internal standard) and 20732–2 (Table 1).

Adopted Solar Wind Mg Fluence

DLC profiles are better than Si (Figures C1 and C5). The solar wind can be measured closer to the surface because of less surface contamination. Transients prior to the onset of steady-state sputtering are minor for DLC, whereas these are quite important for Si. Despite deeper contamination profiles (Figure D1-4), the surface corrections to the DLC solar wind ^{24}Mg depth integrals are smaller (0.9%–2.6% Table D1-4) for DLC than for the Si (6%–8%; Table C2); this in part reflects the much deeper transient depth for Mg in Si than in DLC. There is also some redistribution of Mg (radiation-enhanced segregation; Section C4) in the solar wind Mg depth profile in Si, but there is no evidence that the depth integral is significantly affected.

The 60246 DLC and 60341 Si collector (Appendix C) internal standard samples have a common source of error in the K7A implant fluence; neglecting this, the appropriate error in for the 60341 fluence is 2.8% (average fluence error 0.048; section C12) which is equivalent to 3.3% (Table D2-1-6) for 60246 (average fluence error 0.57). In 1e12 units, the average fluence difference between 60341 and 60246 is 0.037. The *predicted* fluence error difference is 0.074 significantly higher. The average Si-DLC Mg fluence difference is 2.2%. This is the highest precision comparison possible between Si and DLC Mg fluences with present data.

In units of 10^{12} atoms/cm^2, our average adopted fluence from the 60341 Si internal standard Si is 1.698 ± 0.061 (the agreement among the 60341 fluences is anomalously small; we adopt an error of 3.1%; Section C9). The 60341 fluence agrees with the backside depth profiling analysis of Heber et al. (2021) 1.761 ± 0.044. For DLC, omitting 60065, the average of 60246 and 20732–2 is 1.735.(Table 1). The overall average fluence is 1.731×10^{12} atoms/cm^2 for these three results. How to propagate the adopted errors is actually not important because previously neglected common sources of error to Table 1 are more important: 3.5% for the Mg concentration of our NIST glass primary standard (Burnett et al., 2015) and 1.5% for the calibration of our CZ4 primary implant standard. The standard deviation of the above three fluences is 1.8%. The (rms) c 4.2%.

Adopted bulk solar wind Mg fluence: $1.731 \pm 0.073 \times 10^{12}$ atoms/cm^2.

General Comment on Errors

As illustrated by the above, we base our final adopted errors on the reproducibility of fluences from focused studies on different collector materials or different approaches (e.g., internal/external standard). However, in all cases, we have checked to see that the assigned error from a given study is consistent with the estimated analytical errors and made adjustments if necessary (e.g., in the 60341 analyses). Detailed analytical error budgets are given for Mg at the end of Appendices C, D1, and D2-1 and for Fe in Appendices G1, G2, and G3.

FE

Fe Implant Standards

As with Mg, solar wind Fe fluences have been measured using both internal and external standardization. All SW data were processed as matrix-normalized ^{56}Fe profiles. As shown in Figure G2-1, two flight samples of Si and diamond-like-C (DLC), along with control samples and the NIST 617 glass primary standard, were co-implanted with a nominal 10^{12} atoms/cm^2 of ^{54}Fe. A major simplification is that several tests have shown that the implants from Kroko Inc have no measurable inhomogeneities. (<1% in the most precise study of Fe implant sample KB). Thus, all samples on Figure G2-1 have the same implant fluence. The Fe concentration of our NIST 617 glass wafers was independently measured by isotope dilution and solution ICPMS by Humayun at 10.3 ± 0.1 ppm.

SIMS analyses of the NIST 617 glass to calibrate the ^{25}Mg implant fluence presented no problems (Burnett et al., 2015); however, for Fe, problems arose. Fourteen useful profiles were obtained in three separate analysis sessions. A fluence of $5.57 \pm 0.17 \times 10^{11}$ ^{54}Fe atoms/cm^2 is obtained, although four profiles were rejected (Appendix E). As confirmation, a completely independent calibration of the flight implant was carried out based on Si implant sample KB calibrated by Rutherford backscattering at $5.00 \pm 0.05 \times 10^{15}$ ^{56}Fe atoms/cm^2 as a primary standard. As described in Appendix F, flight implant Si control sample CZC was in turn calibrated relative to KB by two different methods: (A) a two-step calibration using an intermediate implant of 3.4×10^{14}/cm^2 and (B) calibrating the ^{54}Fe impurity in KB and calibrating CZC directly relative to it. The A and B pathways agree with a fluence of $5.54 \pm 0.12 \times 10^{11}$ ^{54}Fe atoms/cm^2 which agrees within errors with the fluence measured from the implanted 617 glass (Figure F5).

Fe fluences from Si collectors

(Appendix G1). Seven ^{56}Fe/^{28}Si depth profiles from flight implant sample 60331 were measured in two analytical sessions. Mass scans verified that ^{56}Fe was cleanly resolved from Si_2 (nominal mass resolving power

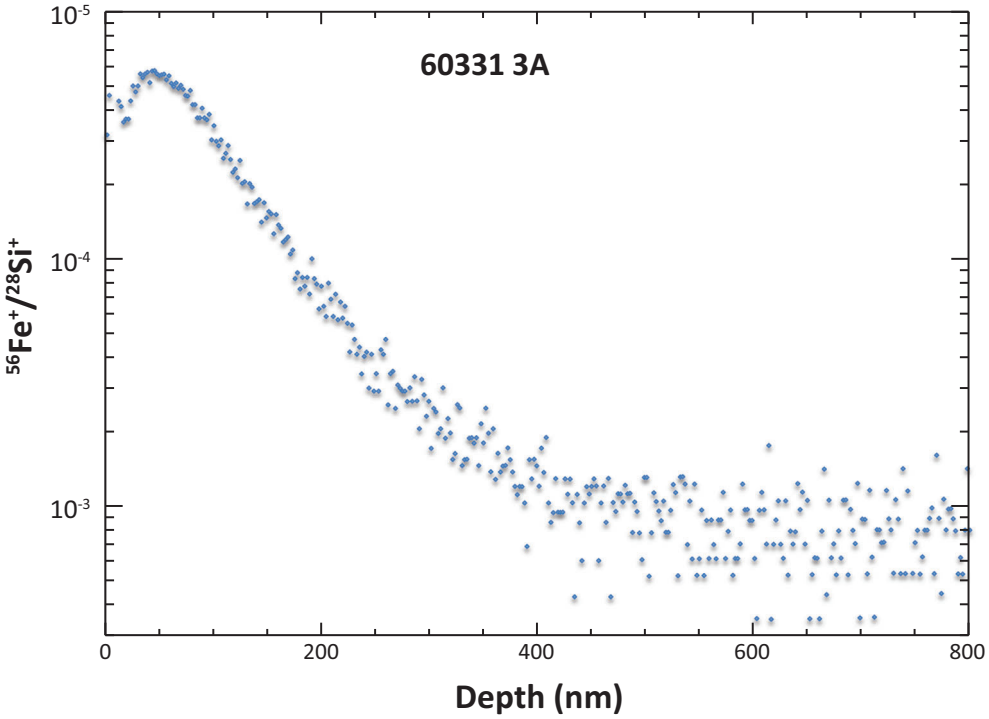

FIGURE 5. ^{28}Si-normalized solar wind ^{56}Fe depth profile in Si. Initial contamination and transients less than for Mg (Figure 1). Background reached beyond 500 nm. Fe fluence based on background-corrected depth integral.

(MRP) 3000–4000). Figure 5 shows a typical measured cps56/^{28}Si profile with good signal/noise and well-defined background as well as adequate resolution of SW ^{56}Fe from contamination and transients (0–20 nm). ^{56}Fe impurities from the ^{54}Fe implant are insignificant, but an approximately 10% correction is required for the flight implant ^{54}Fe due to SW ^{54}Fe (Figure G1-2). As with the same correction to the ^{25}Mg flight implant (Figure 2), errors from this correction are small.

As with Mg (Depth Integrals Section), the background-corrected ^{56}Fe/^{28}Si and ^{54}Fe/^{28}Si integrals are divided into a surface, main, and tail parts. The surface correction is based on fitting the portion of the profile at depths shallower than the peak to a theoretical SRIM profile (e.g., Figures G1-3 and G1-4). Tail refers to the small deep portion of the SW profile unresolved from background. Detailed error analysis for each profile is made with fluence precision ranging from 3.5% to 7.0%.

Figure 6 shows that the individual 60331 profiles all agree with an average value of 1.364×10^{12} Fe atoms/cm^2 with a 1 sigma standard deviation of 2.2%.

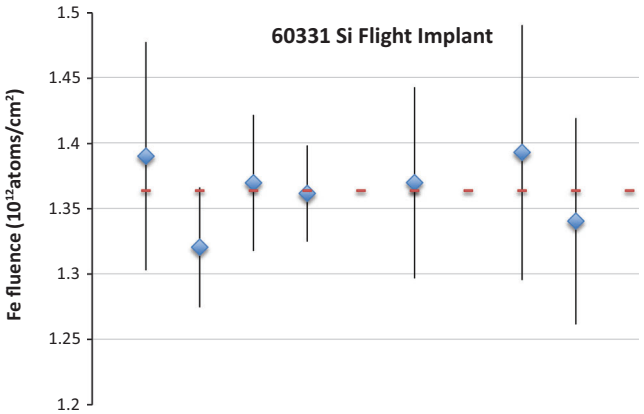

FIGURE 6. The Fe fluences from seven profiles of Genesis Si sample 60331 agree the average value (dashed) within the 1 sigma error bars of the individual analyses. Fe fluences are calculated from the measured ^{56}Fe fluences using the terrestrial ^{56}Fe isotopic abundance

Fe fluences from DLC collectors (Appendix G2)

As with Mg (Figure 4), our initial attempts to measure the SW Fe fluence in DLC collectors showed a lot of scatter due to DLC inhomogeneties (Jurewicz et al., 2021), but precise Mg fluences are obtained with the internal standard implant procedure. Eleven SW ^{56}Fe profiles from DLC samples 60337 and 60246 implanted with ^{54}Fe were processed using the same basic procedures as for Fe in Si collectors (Fe Fluences from Si Collectors Section). The results are given in Figure 7 and Table G2-

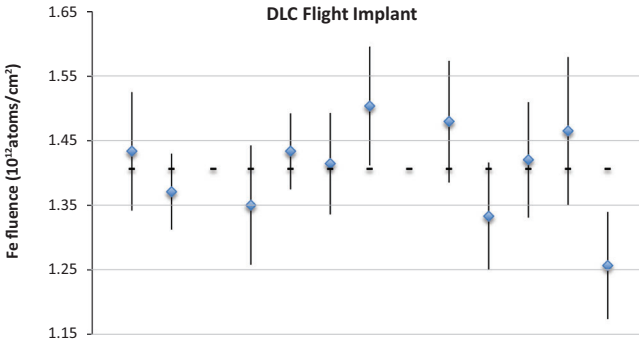

FIGURE 7. Fe solar wind fluence in units of 10^{12} Fe atoms/cm^2 based on DLC collectors. With one exception, the fluences from 11 profiles agree with the average value (dashed) within the 1 sigma error bars of the individual profiles.

TABLE 2. Genesis solar wind Fe fluence summary.[a]

	Fe fluence	Error[b]	No. of profiles
Internal Standard Si[c]	1.364	0.041	7
Internal Standard DLC[d]	1.406	0.078	11
External Standard Si[e]	1.251	0.055	3

[a]Units of 10^{12} atoms/cm^2.
[b]One sigma accuracy estimate; errors of implant standard included.
[c]Sample 60331 (see Appendix G1 for individual profile results).
[d]Samples 60337 and 60246 (see Appendix G2 for individual profile results).
[e]Sample 60490 (see Appendix G3 for individual profile results).

3. Within these errors, all profiles except one agree with the average Fe fluence of $1.406 \pm 0.078 \times 10^{12}$ atoms/cm^2 (Figure 7).

Fe Fluence Summary

Table 2 summarizes the adopted Fe fluence data from the internal standard Si and DLC analyses along with the fluence based on external standard analyses of Sample 64090 (Appendix G3). Errors in Table 2 include the errors from the implant standards thus are our estimate of the accuracy of the measured fluences. As discussed in detail in Appendix G3, the three 64090 profiles are of good quality and fluences agree within the individually estimated errors for individual profiles (Figure G3-8). The standard deviation of the three 64,090 profiles (4.0%) is intermediate between the internal standard Si (2.9%) and DLC (5.6%). For comparison with 64090, (in 10^{12} units), we adopt 1.385 ± 0.059 as the internal standard Si and DLC average. (Here, the error is the Si-DLC average error.) Relative to the formal error in the difference (0.081), the 64090 fluence is lower than the internal standard by 10.7%, 1.7 sigma, marginally significant. The 60490 sample was cleaned with aqua regia with no obvious surface damage, but other flight Si samples were extensively damaged by this treatment. Sample 60490 appears to have some surface loss from the aqua regia treatment (Appendix G3) but the adopted fluence and error allow for this. Nevertheless, the possibility of Fe leaching by aqua regia cannot be ruled out.

External standard Mg fluences were not used in arriving at a final Mg fluence, but errors were large (Table 1). That is not the case for Fe from 64090. Other than the possibility of SW Fe leaching by aqua regia, there is no basis for rejecting the 64090 fluence. A weighted fluence by inverse errors of individual profiles assigns more certainty to the individual profile error estimates than is deserved; however, adopting a fluence weighted by the number of profiles measured seems appropriate and this has been adopted. We adopt the average of Table 2 errors (0.058, 4.2%). This error includes the 64,090 fluence at 2 sigma.

Bulk solar wind Fe fluence: $1.366 \pm 0.058 \times 10^{12}$ atoms/cm^2

DISCUSSION

Solar System Fe/Mg

The interpretable quantity from our Genesis analyses is the bulk solar wind atomic Fe/Mg. Combining the above Fe and Mg fluences:

Bulk SW Fe/Mg: 0.789 ± 0.048.

where the 1 sigma uncertainty (6.0%) is the rms average of the percentage Fe (4.3%) and Mg (4.2%) fluence errors.

Fractionation of the solar wind is primarily between high and low first ionization potential (FIP) elements (e.g., Heber et al., 2021; Laming et al., 2017). Fractionation *among* low FIP (<9 eV) elements is smaller, possibly absent (Heber et al., 2021; Jurewicz et al., 2024; Rieck et al., 2021), but in any case, the FIP for Fe (7.90 eV) and Mg (7.64 eV) are close implying that the measured SW Fe/Mg can be equated with the average solar and thus with the solar system ratio.

Comparison with Photospheric and CI Abundances

Figure 8 shows that the Fe/Mg ratio derived from Genesis samples agrees with these other sources of average solar system Fe/Mg within the quoted 1 sigma errors. Following the arguments in the Introduction, the present uncertainty in the *validity* of the CI Fe/Mg as the solar ratio is not the high accuracy of the analyses (4.1%; Lodders, 2021) but the 11.5% error (Asplund et al., 2021) in the spectroscopic ratio. There is also a lower limit to the validity of CI abundances set by sampling errors and interlaboratory biases

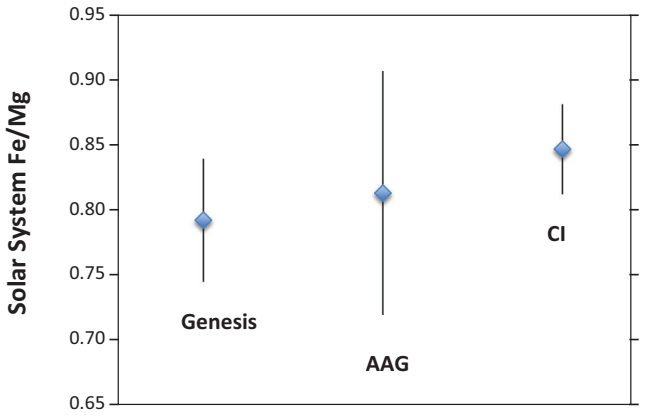

FIGURE 8. Comparison of Genesis Fe/Mg with photospheric spectroscopy (Asplund et al., 2021) and CI carbonaceous chondrites (Lodders, 2021).

(Observational Limits on CI Abundance Validity: Comparison with Ryugu Section). The Genesis Fe/Mg decreases the uncertainty by a factor of about 2 (to 6%). Lodders regards photospheric spectroscopic abundances as generally uncertain to 20%, but we respect the quoted errors of Asplund et al.

Comparison with ACE/SWICS Fe/Mg

Pilleri et al. (2015) reprocessed solar wind abundance data from the SWICS instrument on the ACE spacecraft to match the Genesis collection time interval (The time interval is potentially important as SW abundances could potentially vary with different parts of the solar cycle; however, for low FIP elements, there is no evidence of this at present). Pilleri et al. report abundances relative to Mg and relative to the photosphere spectroscopic Fe/Mg. For completeness, we convert their abundances to the Asplund et al.'s (2021) Fe/Mg ratio of 0.813, instead of the 0.794 used by Pilleri et al., although this makes negligible difference. The SWICS bulk solar wind $Fe/Mg = 1.00 \pm 0.21$ is 26% higher (1.2 sigma) than the Genesis ratio. SWICS Fe/Mg ratios for the Genesis SW *regimes* (Burnett, 2013) are all higher than the Asplund et al.'s 0.813, but not outside of error limits. The SWICS Fe/Mg for the Genesis period low speed (L) (Interstream) regime is significantly higher than the Genesis period high speed (H) (Coronal hole) solar wind by 19%. Pilleri et al. interpret this and an overall speed dependence of Fe/Mg, as evidence that solar wind elemental fractionations are not determined by FIP alone. This is important because it would significantly complicate the interpretations of this paper. However, the 19% is surprising because the regime, Mg-normalized abundances for Ca, Al, and Na are agree to within 2% *precision* for all three of the Genesis regime samples (Heber et al., 2021). The 19% L/H Fe difference can be tested by Genesis regime sample analysis.

Observational Limits on CI Abundance Validity: Comparison with Ryugu

The CI abundance uncertainties, set by sampling and interlaboratory bias (e.g. Palme et al., 2014), are unlikely to be improved (at least for Fe and Mg) by new/better analytical techniques. As emphasized by Palme et al. (2014), the present CI abundances are based on the average of a large number of analyses, but from only two meteorites, Orgueil and Ivuna. The best constraint on CI sampling errors comes from Barrat et al. (2012) who document significant variations. Rejecting one outlier sample, 19/46 elements have ≥5% differences for gram-sized samples from six different large Orgueil stones.

The validity of CI abundances can be tested by new samples, but the Earth's atmosphere presents a significant barrier for recovery of friable CI meteorites. Carbonaceous asteroidal sample returns offer a new dimension.

The returned samples from asteroid Ryugu are CI-like material. Independent elemental analyses of different samples are available from Yokoyama et al. (2022) and Nakamura et al. (2022). There is a general consensus (e.g., Alfing et al., 2019; Barrat et al., 2012; Morlock et al., 2006; Palme et al., 2014) that gram-sized samples of CI are required to get a representative average; consequently, allocation of sufficiently large Ryugu samples for bulk analysis to obtain significant constraints on the validity of CI abundances should not be possible, given the 5.4 g sample returned. The Ryugu data suggest otherwise. The Hayabusa 2 mission collected two samples (TD1 and TD2) separated by 100' s of meters on Ryugu; these are equivalent to two separate CI samples, except for the important distinction that they are known to come from the same asteroid. Yokoyama et al. analyzed approximately 25 mg samples from each site. Nakamura et al. made separate analyses of 16 sub-mg samples, a total mass of 4.4 mg. The atomic Fe/Mg for Yokoyama et al. ($0.819 \pm 6\%$ TD1-TD2 difference) and Nakamura et al. ($0.813 \pm 8\%$ TD1-TD2 difference) agree well and with the data in Figure 8.

A significant difference between Ryugu and classical CI is the abundances of "coarse" grains (> micron size) of some minerals. Apatite is especially important as the host phase of many lithophile elements, and the Ryugu apatite modal abundances (Nakamura et al) are over an order of magnitude greater than Orgueil (Alfing et al., 2019); probably because the Ryugu data have a lower grain size cutoff (Appendix I).

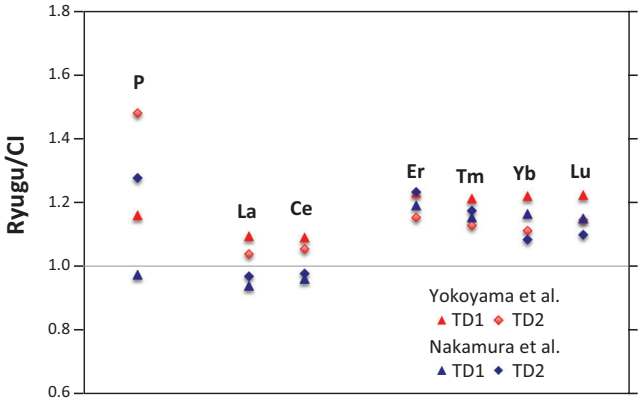

FIGURE 9. Comparison of Mg-normalized Ryugu/CI abundances for P, LREE (La, Ce), and HREE (Er, Tm, Yb, Lu) from Yokoyama et al. (2022) and Nakamura et al. (2022) and for the two Ryugu sampling sites (TD1 and TD2). Details in Appendix I. Despite small sample sizes, Ryugu data are very consistent for the REE. Larger P variations reflect variations in apatite abundance.

We have not made a detailed study of the published Ryugu elemental analyses; however, the data suggest a possible significant difference in REE from that those in CIs. Consequently, in Appendix I, we have made a close comparison of Ryugu and CI, summarized in Figure 9 for Mg-normalized abundances of P, LREE, and HREE. Following Harold Urey, the Mg normalization minimizes the effects of differences in water and C concentrations. Interlaboratory bias should be eliminated in separate TD1 versus TD2 comparisons for Yokoyama et al. and Nakamura et al. Serious sampling errors from the small samples analyzed would produce scatter in Figure 9, but this appears relatively small. The requirement of gram-sized samples of Orgueil to get accurate abundances may not apply to the elements considered here. Or possibly, despite larger abundances of coarse mineral grains, Ryugu may be overall more homogeneous. If the Yokoyama data, based on an order of magnitude larger sample size, are adopted, the average Mg-normalized Ryugu/CI ratios are 1.27 ± 0.11 for P, 1.07 ± 0.03 for the LREE, and 1.18 ± 0.05 for the HREE (Table I4), where the errors are the TDI-TD2 differences from the average. Overall, the Ryugu results are remarkably consistent, despite the small samples, especially for the REE.

It is possible that the REE pattern and P abundance in Ryugu are different from CI. Two independent analyses (Appendix I) are used for Figure 9 which minimizes the effect of interlab bias; however, both sets are based on ICPMS analyses. The Ryugu/CI differences in Figure 9 require confirmation, but these illustrate a major issue. When two CI-like samples differ significantly, in this case 7%–27%, which is solar?

TABLE 3. C chondrite Fe/Mg and variations.

Group	# falls	Atomic <Fe/Mg>	Standard deviation	Standard deviation (%)
Chondrite				
CI	3	0.851	0.011	1.3
CM	10	0.775	0.016	2.1
C3V	4	0.697	0.005	0.7
C3O	5	0.755	0.025	3.3
Genesis				
G − 1σ		0.743		
G + 1σ		0.839		

Comparisons with Chondrite Fe/Mg

Having solar composition for any meteorite is important, even for a limited group of elements or a single important ratio like Fe/Mg, because this shows that at least part of this material has not had significant fractionation from the average composition of the solar nebula. Only CIs have near-solar composition for volatile elements like S (e.g. Palme et al., 2014), but even here, the qualification "only for non-volatile elements" must be added with "non-volatile" inferred from the data. With more valid solar abundances, it is possible to investigate the issue of whether specific C groups, or individual meteorites, have solar composition at a higher level of precision. Identifying those groups or meteorites that do not have solar composition potentially provides clues to previously unrecognized or poorly understood nebular processes and/or structure.

The variations of average C group Mg/Si ratios (including CI) are remarkably small, only 6% (fig. 1 of Palme et al., 2015). However, for Fe/Mg, the range appears larger: 30% (fig. 3 Palme et al., 2015), a variation significantly larger than the errors in the Genesis Fe/Mg, which in turn agrees with the CI ratio (Figure 8). We compare literature whole rock Fe/Mg analyses of carbonaceous chondrites with the Genesis bounds on the solar Fe/Mg, a comparison now valid at the ≈10% accuracy level. Table 3 shows our C chondrite group averages of Fe/Mg. We restrict the comparison to falls in order to recognize anomalous meteorites and focus as much on variations as on group averages. The input data to Table 3 are individual meteorite Fe/Mg, averaging data from different laboratories. Details are given in Appendix J. The intermeteorite % standard deviations in Table 3 are small, and intergroup differences in Fe/Mg are clearly resolved with $CI > CM \cong C3O > C3V$. This has been noticed before (e.g., Hezel et al., 2018; Kallemeyn & Wasson, 1981) but not elaborated upon.

The small variations in the C chondrite group individual meteorite averages indicate homogeneous

parent bodies; this conclusion applies to a major component (C-type) of the asteroid belt. The Aguas Zarcas C chondrite breccia appears an exception. It is possibly of great importance that it contains many "non-group" C chondrite clasts (Kerrouch et al., 2022).

The CM average and standard deviation in Table 3 exclude Haripura for which a single analysis gives a highly anomalous Fe/Mg = 1.95 (Table J3). Haripura appears to be a typical CM (Metzler et al., 1992), but may be worthy of further attention.

Tables J2 and J3 indicate that C chondrite interlaboratory bias and sampling errors for Fe/Mg are small, less than about 5%. The intermeteorite standard deviations in Table 3 are smaller, suggesting convergence in the group means.

Comparison of the Genesis 1 sigma limits on solar Fe/Mg (Table 3) shows CI chondrites at the +1 sigma limit. All nine CM meteorites (excluding Haripura) have Fe/Mg within the Genesis 1 sigma range (Table J3). The five C3O meteorites have Fe/Mg near the Genesis −1 sigma limit and the four C3V meteorites are consistently below the Genesis −1 sigma limit. If we adopt 2 sigma standards, all these C chondrites could have solar Fe/Mg. All C chondrites appear to have the same Mg/Si as well (e.g., Palme et al., 2014, 2015). Variations in Ca/Si and Al/Si and presumably other refractory lithophile elements reflect CAI components (e.g., Palme et al., 2014; Wasson, 1974, fig. II-2).

Despite complications, meteorites with near solar Mg, Fe, and Si abundances place a major constraint on nebular source regions. The small variations in C chondrite group Fe/Mg probably reflect a small amount of metal–silicate fractionation, but considering this is beyond the scope of this paper.

SUMMARY

Solar wind Fe/Mg is a more valid measure of solar composition than CI chondrites and can be measured more accurately than spectroscopic photospheric abundances. Fe is an element of high cosmochemical importance, with Fe/Mg (as well as oxidation state) controlling the densities of the terrestrial planets. SIMS analyses of Mg and Fe fluences made in four different laboratories and two different Genesis collector materials give satisfactory agreement. Both Si and diamond-like-C collectors give high signal to noise depth profiles for Mg (Figures 1 and C5) and Fe (Figures 5 and G2-3). Si and DLC fluences agree for both elements. The Mg fluence is $1.731 \pm 0.073 \times 10^{12}$ atoms/cm^2. The Fe fluence is $1.366 \pm 0.058 \times 10^{12}$ atoms/cm^2. To obtain the highest accuracy, all plausible sources of error down to the 1% level were investigated and documented in supporting online appendices.

Our value for the solar system Fe/Mg atomic ratio, 0.789 ± 0.048 agrees at 1 sigma with spectroscopic photospheric abundances with CI chondrite abundances (Figure 8) and with the solar wind data from the ACE spacecraft (Comparison with ACE/SWICS Fe/Mg Section). Following the above arguments, the present uncertainty in the *validity* of the CI Fe/Mg is not the high accuracy of the analyses (4.1%; Lodders, 2021) but the 6% error in the Genesis solar Fe/Mg.

CI-like samples from asteroid Ryugu give Fe/Mg in agreement with Genesis and meteoritic CI samples, despite very small sample sizes. Confirmation is required, but differences in P abundances and REE patterns between Ryugu and CI (Figure 9) suggest the possibility of 10%–30% differences. Independently, depletions of 10%–20% in CI abundances relative to the photosphere have been documented by Asplund et al. (2021) and Jurewicz et al. (2024). Element by element comparisons are required, but 10%–30% limits to the validity of CI abundances are likely. This level of uncertainty is acceptable for many applications and CI composition as a source of solar abundances should continue to be used, but their limitations should be recognized.

Regardless of possible Ryugu-CI differences, the true uncertainty in the validity of CI abundances as average solar composition is not given by the small analytical or sampling errors in the CI-like sample data; the ultimate uncertainty in validity is the errors in the photospheric abundances.

The higher accuracy of the Genesis solar Fe/Mg permits a comparison with chondritic Fe/Mg at the 10% level. Using only data on falls to permit close comparison, Table 3 shows that intermeteorite Fe/Mg averages differ for the main C chondrite groups but are all within, or very close to, the ±1 sigma Genesis solar Fe/Mg. Variations in the individual meteorite Fe/Mg for a single C chondrite group are small indicating homogeneous parent bodies, at least for Fe/Mg.

Acknowledgments—This research was supported by NASA LARS grants, specifically 80NSSC22K0589 (Jurewicz, Burnett). Helpful reviews were received by Andrew Westphal and an anonymous reviewer. Our success was based on all those who contributed to the Genesis mission, and especially Judy Allton, Carla Gonzales, and the JSC Genesis Curation Facility. We thank Denton Ebel for the use of his chondrite database.

Data Availability Statement—The data that support the findings of this study are available in the Appendices, or on request from the corresponding author. The data are not publicly available due to privacy or ethical restrictions.

Editorial Handling—Dr. Jull Timothy

REFERENCES

Alfing, J., Patzeck, M., and Bischoff, A. 2019. Modal Abundances of Coarse-Grained (>5 μm) Components within CI Chondrites and their Individual Clasts – Mixing of Various Lithologies on the CI Parent Body(ies). *Geochemistry* 79: 125532.

Asplund, M., Amarsi, A. M., and Grevesse, N. 2021. The Chemical Makeup of the Sun: A 2020 Vision. *Astronomy and Astrophysics* 653: A141–A171.

Barrat, J. A., Zanda, B., Monyier, F., Bollinger, C., Liorzou, C., and Bayon, G. 2012. Geochemistry of CI Chondrites: Major and Trace Elements, and Cu and Zn Isotopes. *Geochimica et Cosmochimica Acta* 83: 79–92.

Burnett, D. S. 2013. The Genesis Solar Wind Sample Return Mission: Past, Present, and Future. *Meteoritics & Planetary Science* 48: 2351–70.

Burnett, D. S., Jurewicz, A. J. G., and Woolum, D. S. 2019. The Future of Genesis Science. *Meteoritics and Planetary Science* 54: 1092–1114.

Burnett, D. S., Jurewicz, A. J. G., Woolum, D. S., Wang, J., Paque, J. M., Nittler, L. R., McKeegan, K. M., et al. 2015. Ion Implants as Matrix-Appropriate Calibrators for Geochemical Ion Probe Analysis. *Geostandards and Geoanalytical Research* 39: 265–276.

Heber, V. S., McKeegan, K. D., Burnett, D. S., Duprat, J., Guan, Y., Jurewicz, A. J. G., Olinger, C. T., and Smith, S. P. 2014. Accurate Analysis of Shallowly Implanted Solar Wind Ions by SIMS Backside Depth Profiling. *Chemical Geology* 390: 61–73.

Heber, V. S., McKeegan, K. D., Steele, R. C. J., Jurewicz, A. J. G., Rieck, K. D., Guan, Y., Wieler, R., and Burnett, D. S. 2021. Elemental Abundances of Major Elements as Measured in Genesis Targets and Implications on Solar Wind Fractionation. *The Astrophysical Journal* 907: 1–16.

Hezel, D. C., Bland, P. A., Palme, H., Jacquet, E., and Bigolski, E. 2018. Composition of Chondrules and Matrix and their Complementary Relationship in Chondrites. In *Chapter 4: Chondrules: Records of Protoplanetary Disk Processes*, edited by S. S. Russell, H. C. Connolly, Jr., and A. N. Krot. Cambridge, England: Cambridge University Press.

Jurewicz, A. J. G., Amarsi, A. M., Burnett, D. S., and Grevesse, N. 2024. Differences in Elemental Abundances Between CI Chondrites and the Solar Photosphere Accepted for Publication in Meteoritics and Planetary Science. *Meteoritics and Planetary Science* 59: 3193–3214. https://doi.org/10.1111/maps.14272.

Jurewicz, A. J. G., Burnett, D., Rieck, K., Hervig, R., Friedmann, T., Williams, P., Daghlian, C., and Wiens, R. 2017. Understanding Heterogeneity in Genesis Diamond-like Carbon Film Using SIMS Analysis of Implants. *Journal of Materials Science* 52: 11282–305. https://doi.org/10.1007/s10853-017-1267-3. (Open Access Paper).

Jurewicz, A. J. G., Burnett, D. S., Rieck, K. D., Hervig, R., Huss, G., Wiens, R. C., Laming, J. M., and Wadhwa, M. 2020. Mg Isotopes in the Bulk Solar Wind as Determined from Genesis DoS Collectors. *Meteoritics and Planetary Science* 55: 352–375.

Jurewicz, A. J. G., Burnett, D. S., Wiens, R. C., Friedmann, T. A., Hays, C. C., Hohlfelder, R. J., Nishiizumi, K., et al. 2003. The Genesis Solar-Wind Collector Materials. *Space Science Reviews* 105: 535–560.

Jurewicz, A. J. G., Olinger, C. T., Burnett, D. S., Guan, Y., Hervig, R., Rieck, K. D., and Woolum, D. S. 2021. Quantifying Low Fluence Ion Implants in Diamondlike Carbon Film by Secondary Ion Mass Spectrometry by Understanding Matrix Effects. *Journal of Analytical Atomic Spectrometry* 36: 194–209.

Kallemeyn, G. W., and Wasson, J. T. 1981. The Compositional Classification of Chondrites I. The Carbonaceous Chondrite Groups. *Geochimica et Cosmochimica Acta* 45: 1217–30.

Kerrouch, I., Kebukawa, Y., Bischoff, A., Zolensky, M. E., Wölfer, E., Hellmann, J. L., Ito, M., et al. 2022. Heterogeneous Nature of the Carbonaceous Chondrite Breccia Aguas Zarcas – Cosmochemical Characterization and Origin of New Carbonaceous Chondrite Lithologies. *Geochimica et Cosmochimica Acta* 334: 155–186.

Laming, J. M., Heber, V. S., Burnett, D. S., Guan, Y., Hervig, R., Huss, G. R., Jurewicz, A. J. G., et al. 2017. Determining the Elemental and Isotopic Composition of the Pre-Solar Nebula from Genesis Data Analysis: The Case of Oxygen. *Astrophysical Journal Letters* 851: L12–L18.

Lodders, K. 2021. Relative Atomic Solar Abundances, Mass Fractions, and Atomic Masses of the Elements and their Isotopes, Compositions of the Solar Photosphere, and Compositions of the Major Chondrite Groups. *Space Science Reviews* 217: 43–77.

McSween, H. Y. 1993. Cosmic or Cosmuck? *Meteoritics* 28: 3–4.

Metzler, K., Bischoff, A., and Stoffler, D. 1992. Accretionary Dust Mantles in CM-Chondrites: Evidence for Nebula Processes. *Geochimica et Cosmochimica Acta* 56: 2873–97.

Morlock, A., Bischoff, A., Stephan, T., Floss, F., Zinner, E., and Jessberger, E. K. 2006. Brecciation and Chemical Heterogeneities of CI Chondrites. *Geochimica et Cosmochimica Acta* 70: 5371–94.

Nakamura, E., Kobayashi, K., Tanaka, R., Kunihiro, T., Kitagawa, H., Potiszil, C., et al. 2022. On the Origin and Evolution of the Asteroid Ryugu. A Comprehensive Geochemical Perspective. *Proceedings of the Japan Academy of Sciences* B98: 227–282.

Olinger, C. T., Dragland, E. J., and Martino, A. J. 2018. Interpreting Measured Genesis Solar Wind Profiles through Simulation. *49th Lunar and Planetary Science Conference*, abstract #2861.

Palme, H., Hezel, D. C., and Ebel, D. S. 2015. The Origin of Chondrules: Constraints from Matrix Composition and Matrix-Chondrule Complementarity. *Earth and Planetary Science Letters* 411: 11–19.

Palme, H., Lodders, K., and Jones, A. 2014. Solar System Abundances of the Elements. In *Chapter 2.2 in Treatise on Geochemistry*, edited by A. Davis, 2nd ed., vol. 1. Amsterdam, Netherlands: Elsivier.

Pilleri, P., Reisenfeld, D. B., Zurbuchen, T. H., Lepri, S. T., Shearer, P., Gilbert, J. A., von Steiger, R., and Wiens, R. C. 2015. Variations in Solar Wind Fractionation as Seen by ACE/SWICS and the Implications for GENESIS Mission Results. *The Astrophysical Journal* 812: 1–10.

Rieck, K. D., Jurewicz, A. J. G., and Ogliore, R. C. 2021. Comparing SIMS Data For Solar Wind Na in Two Collectors Using Multiple Approaches. *52nd Lunar and Planetary Science Conference, abstract #2638*.

Wasson, J. 1974. *Meteorites*. Berlin: Springer-Verlag.

Wilson, R. G., Stevie, F. A., and Magee, C. W. 1989. *Secondary Ion Mas Spectrometry*. New York: Wiley.
Yokoyama, T., Nagashima, K., Nakai, I., Young, E. D., Abe, Y., Aléon, J., Alexander, C. M. O'D., et al. 2022. Samples Returned from the Asteroid Ryugu are Similar to Ivuna-Type Carbonaceous Meteorites https://doi.org/10.1126/science.abn7850.
Ziegler, J. F., Ziegler, M. D., and Biersack, J. P. 2010. SRIM—The Stopping and Range of Ions in Matter. *Nuclear Instruments and Methods in Physics Research Section B* 268: 1818–23.

SUPPORTING INFORMATION

Additional supporting information may be found in the online version of this article.

Appendix A. Appendix List.

Appendix B. Implant Standards Used.

Appendix C. Mg/Si Data Processing.

Appendix D1. Mg in DLC. Sample 20732-2.

Appendix D2. 1. DLC Internal Standard Analyses, sample 60246.

2. DLC External Standard Analyses, sample 60065, session D.

Appendix E. Calibration of ^{54}Fe flight Implant with NIST 617 glass.

Appendix F. ^{54}Fe flight Implant Calibration with High Fluence KBSi Implant.

Appendix G1. Fe Fluence from Si Collectors Internal Standard.

Appendix G2. Solar Wind Fe Fluence in DLC based on ^{54}Fe Flight Implant.

Appendix G3. Fe in Si External Standard.

Appendix H. Rastered Beam Deadtime.

Appendix I. Ryugu – CI Comparisons.

Appendix J. Genesis – Chondrite comparisons.